Imlunestrant a next-generation oral SERD overcomes *ESR1* mutant resistance in estrogen receptor-positive breast cancer

Shira Sherman[1*], Zachary M. Sandusky[1,2*], Douglas Russo[1,3,4], David Zak[5], Agostina Nardone[1], Delia Friel[1,2], Francisco Hermida Prado[1], Capucine Heraud[1], Genevra Kuziel[1], Ana Verma[3,6,7], Giorgio Gaglia[3,6,7], Sheheryar Kabraji[1,3,8] Quang-De Nguyen[9], Sandro Santagata[3,6,7], Sean W. Fanning[5], Rinath Jeselsohn[1,2,3,8#]

[1]Department of Medical Oncology, Dana-Farber Cancer Institute, Boston, MA, USA

[2]Center for Functional Cancer Epigenetics, Dana-Farber Cancer Institute, Boston, MA, USA

[3] Harvard Medical School, Boston, MA, USA

[4] Department of Data Science, Dana-Farber Cancer Institute, Boston, MA, USA

[5]Department of Cancer Biology, Loyola University Stritch School of Medicine, Maywood, IL, USA

[6]Ludwig Center at Harvard, Harvard Medical School, Boston, MA, USA

[7]Department of Pathology, Brigham and Women's Hospital, Harvard Medical School, Boston, MA USA

[8]Susan F. Smith Center for Women's Cancers, Dana-Farber Cancer Institute, Boston, MA, USA

[9]Lurie Family Imaging Center, Center for Biomedical Imaging in Oncology, Dana-Farber Cancer Institute, Boston, MA, USA

* Equal contribution

[#] Corresponding author and lead contact:

Rinath Jeselsohn, MD PhD; Dana-Farber Cancer Institute, 450 Brookline Ave, Boston, MA 02215, USA.

E-mail: Rinath_jeselsohn@dfci.harvard.edu

Abstract

Estrogen receptor alpha (ER) is a critical driver of tumorigenesis and tumor progression in most breast cancers. Endocrine therapies (ET) targeting ER are central to treating hormone receptor-positive breast cancer (BC), but resistance poses a clinical challenge. Some resistance mechanisms, particularly those involving estrogen-independent activity such as the *ESR1* mutations, rely on ER signaling, supporting the need for next-generation ET. We investigated the preclinical efficacy of imlunestrant, an oral selective ER degrader, in ER-positive BC pre-clinical models, including models harboring the Y537S *ESR1* mutation, an activating mutation. Imlunestrant demonstrated antagonistic activity and effective degradation of both wild-type and mutant ER, resulting in cell growth suppression. In vivo, imlunestrant outperformed fulvestrant leading to tumor regression in a patient derived xenograft harboring the Y537S *ESR1* mutation. Cyclic mutiplexed immunofluorescence and transcriptomic analysis revealed enhanced cell cycle arrest and downregulation of estrogen-responsive genes with imlunestrant treatment. Additionally, a genome wide CRISPR knock-out screen identified several vulnerabilities that were either persistent or gained after imlunestrant treatment, providing a rationale for future studies of combination treatments with imlunestrant. Collectively, these results highlight the on-target and selective activity of imlunestrant, which can circumvent resistance engendered by the Y537S *ESR1* mutation.

Keywords: imlunestrant; breast cancer; estrogen receptor positive; selective estrogen receptor degrader; ESR1 mutation

Introduction

Estrogen receptor alpha (ER) is a nuclear hormone receptor and a key driver of tumorigenesis and tumor progression in most breast cancers. Estrogen binding to ER leads to its activation, a process that involves ER dimerization, phosphorylation, and translocation to the nucleus where ER binds to co-factors and chromatin at estrogen response elements (ERE) sites and directly mediates the transcription of hundreds of genes. The transcriptional activity of ER is dictated by other transcription factors, such as the pioneer transcription factor FOXA1, and is tightly regulated by co-regulators that either activate or repress ER activity (1, 2).

Endocrine therapy that targets ER is the mainstay treatment in hormone receptor-positive (HR+) breast cancers, which express ER and/or the progesterone receptor (PR). There are several classes of endocrine therapies, including selective estrogen receptor modulators (SERMs), such as tamoxifen, aromatase inhibitors that suppress the conversion of androgens to estrogen and production of estrogen from peripheral tissue, selective estrogen receptor degraders (SERD) that are pure ER antagonists and enhance the proteasomal degradation of ER, and suppression of ovarian estrogen production in pre-menopausal women with GNRH analogs or bilateral salpingo-oophorectomy. Currently, the only SERD that is approved for all patients with metastatic HR+ breast cancer is fulvestrant. Although endocrine therapy has a substantial impact on outcomes in early and advanced stages of HR+ breast cancer, endocrine resistance is a major clinical obstacle. Multiple mechanisms of endocrine resistance exist, and several are unique to a specific class of endocrine therapy (3). As an example, the agonistic activity that drives resistance is unique to tamoxifen and in the clinic is evidenced by the tumor response detected after tamoxifen withdrawal (4).

Estrogen independent activity of ER is a mechanism of resistance that is more specific to aromatase inhibitors. Several studies have shown that the crosstalk between ER and receptor tyrosine kinase signaling followed by activation of the PI3Kinase-AKT-MTOR and MAPK pathways results in estrogen independent phosphorylation and activation of ER (5, 6). *ESR1* ligand binding missense mutations are predominantly acquired during treatment with aromatase inhibitors in metastatic disease, and after such treatment in metastatic disease these alterations are detected in up to above 50% of patients when testing circulating tumor DNA (ctDNA) (7). These mutations, especially Y537S, reduce binding affinities of SERMs and SERDs while also impairing their abilities to engage the therapeutic conformation of the ligand binding domain (8-10). Overall, in pre-clinical studies the Y537S *ESR1* mutation was found to possess the most potent resistance to ER antagonists and ligand independent activity (11). Clinical observations further support the relative resistance to fulvestrant in the presence of a Y537S *ESR1* mutation (12), which is likely attributed to the poor bioavailability of this drug coupled to the increased quantities required to saturate the mutant receptor (13).

Pre-clinical studies have shown that *ESR1* mutations have neomorphic properties that promote a metastatic phenotype and targeting these mutations leads to metastatic regression (14). Thus, *ESR1* mutations are a biomarker of an active but altered ER axis and a therapeutic target. Taken together, the high prevalence of these mutations and their biological implications warrant the development of novel endocrine therapies that have superior pharmacokinetics and/or better affinity mutant ER capable of destabilizing wild type (WT) and mutant ER. Recently, elacestrant, a next-generation endocrine therapy with SERD activity was approved for the treatment of *ESR1* mutant metastatic breast cancer (15). Additionally, there are several other novel endocrine therapies in clinical development (16). Imlunestrant is a novel SERD in clinical development with an excellent safety profile and a strong signal

of activity in metastatic HR+ breast cancer (17, 18). In this study, we investigated the preclinical anti-cancer activities of imlunestrant with an emphasis on its effectiveness in the presence of the Y537S *ESR1* mutation.

Results

Imlunestrant has pure antagonistic activity and is a potent degrader of mutant ER

To characterize the preclinical activity of imlunestrant, we used MCF7 and T47D ER+ breast cancer model cell lines without and with doxycycline (DOX) induction of the Y537S *ESR1* mutation (14). We first evaluated the activity of imlunestrant on cell growth and observed dose dependent growth suppression with significant activity at a concentration of 1nM. The IC50 concentrations were 0.34nM and 5.2nM in T47D and MCF7 cells, respectively, which were lower compared to fulvestrant (fulvestrant IC50 was 2.2 and 19 in T47D and MCF7 cells, respectively) (Figure 1A-B and Supplemental Figure 1A-C). Off target effects were assessed in the triple negative breast cancer cell line, MDAMB231, in which imlunestrant did not affect cell proliferation (Supplemental Figure 1D). Given the importance of the pure antagonistic activity of a SERD, we tested the effects of imlunestrant in MCF7 cells overexpressing ERE-luciferase in apo and ligand bound states (Figure 1C-E). We observed strong antagonistic activity of imlunestrant in E2 treated conditions already after 6 hours of treatment, without evidence of agonistic activity in both states when testing imlunestrant at a concentration up to 1,000 nM and up to treatment for 24 hours. Similar results were seen with fulvestrant (Supplemental Figure 1F). In aggregate, these results indicate that imlunestrant is an ER antagonist without agonistic activity in breast cancer cells.

Next, we examined the ability of imlunestrant to degrade WT and Y537S ER by immunoblotting. Initial degradation of WT-ER was observed as early as 6 hours with the magnitude of ER degradation

continuously increasing up to 48 hours and retained at 72 hours. Although at 24 hours the degradation of WT-ER was overall comparable between fulvestrant treatment and imlunestrant, mutant ER protein degradation was superior with imlunestrant treatment versus fulvestrant (Figure 1F-G). Furthermore, mutant ER degradation persisted beyond 24 hours with imlunestrant treatment. Despite the evidence of mutant and endogenous WT- ER degradation by imlunestrant and fulvestrant within 24 hours, the dose response curves of imlunestrant and fulvestrant on day 5 shifted with the expression of the Y537S ER mutations (Figure 1B and Supplemental Figure 1A-C). Longer term in vitro experiments with colony assays of WT and mutant ER cells showed that at day 14 higher concentrations of imlunestrant were able to suppress cell confluency in the presence of the ER mutation (Figure 1H-I). Taken together, these in vitro studies suggest that imlunestrant effectively degrades mutant ER, however, the ER mutations likely diminish the antagonistic activity of imlunestrant and this can be circumvented by a higher concentration.

To test for the selective activity of imlunestrant on transcription in a non-biased genome wide manner, we performed RNAseq experiments in hormone deprived conditions without and with the induction of the Y537S ER mutation. The DOX-inducible cells were cultured in hormone deprived (HD) conditions for 3 days and then treated with either vehicle (DMSO), E2, imlunestrant or fulvestrant for 6 and 12 hrs. In addition, cells were first stimulated with DOX to induce the Y537S ER mutation followed by culture in HD conditions and then treatment with DMSO, imlunestrant or fulvestrant for 6 and 12 hrs (Figure 2A and Supplemental Table 1). As expected, E2 treatment of HD cells led to significant transcriptional changes, including the upregulation of canonical ER transcriptional targets (Figure 2B). In addition, induction of the Y537S ER mutation in HD conditions resulted in significant gene expression changes, including canonical ER transcription targets among other genes (Figure 2B), as we previously described (14). We next tested the transcriptional effects of imlunestrant and fulvestrant. In cells with WT-ER after

culture in HD conditions, imlunestrant and fulvestrant had no transcriptional effects since ER is inactive in these conditions, highlighting the specificity of these two ER antagonists. In contrast in MCF7 and T47D cells expressing the Y537S ER mutation in HD conditions, imlunestrant and fulvestrant treatment resulted in significant transcriptional changes, including the down regulation of genes of the estrogen response and cell cycle pathways (Figure 2D-E and Supplemental Figure 2A-D and Supplemental Table 2). Overall, when comparing the pathways modulated by imlunestrant and fulvestrant treatment at 6 and 12 hrs in MCF and T47D cells expressing the Y537S ER mutation in HD conditions, we observed comparable effects. Both drugs led to the downregulation of expected pathways, such as estrogen response early and late, E2F targets, G2M checkpoint and MYC targets (Figure 2F). In aggregate, our results revealed highly selective on-target activity of imlunestrant in the presence of WT and mutant ER.

Increased cell cycle arrest results in superior suppression of tumor growth

To evaluate the in vivo activity of imlunestrant, we turned to a PDX model derived from a liver metastasis from a patient who was heavily pre-treated. This PDX has high ER expression, harbors a Y537S *ESR1* mutation, and is E2 independent (19). As shown in Figure 3A, the tumors were resistant to fulvestrant but were highly sensitive to imlunestrant. Already at day 10, treatment with imlunestrant as a single agent led to significant tumor regression, which persisted until the end of the experiment at day 28. The mice tolerated imlunestrant treatment well without a significant weight change (Figure 3B). In line with the tumor growth results, ER, PR and Ki67 levels were significantly lower in tumors treated with imlunestrant compared to fulvestrant and vehicle control at day 10 (Figure 3C-F). Although, at day 28, in the residual tumors, ER levels were marginally higher in imlunestrant compared to fulvestrant treatment, Ki67 levels remained significantly lower with imlunestrant treatment (Figure 3G-J).

Next, we performed multiplexed immunofluorescence to calculate the Multivariate Proliferation Index (MPI) on PDX tumors harvested after treatment for 10 days (an early time point to assess direct effects) and 28 days. MPI is calculated based on expression of several distinct proliferative markers, including Ki67, PCNA, MCM2, and the two markers of cell-cycle arrest p21, p27. MPI classifies each cell as either proliferative, if the cell expresses a positive balance of the proliferation markers, non-proliferative for a cell that lacks the expression of proliferative markers, and arrested if the cell expresses one or two of the cell-cycle arrest markers, irrespective of the expression of the proliferation markers, providing a comprehensive measure of the tumor proliferation state at the single cell level (20). Imlunestrant treatment resulted in a significantly greater suppression of Ki67 and phospho-Rb compared to fulvestrant. Remarkably, on days 10 and 28, the percentage of proliferating cells was significantly decreased by imlunestrant, the non-proliferating tumor cells (Ki67- and phospho-Rb-) were significantly increased, and there was no impact of treatment on percentage of arrested cells (Figure 4A-D). To further investigate the impact of imlunestrant on the cell cycle, the distribution of the cells was separated by pseudotime. In vehicle treated tumors, the cells are equally distributed across the cell cycle in pseudotime. While fulvestrant treatment partially suppressed cell cycle progression, imlunestrant nearly completely blocked the cell cycle and cells accumulated in one area of pseudotime, which is most consistent with the G1 cell cycle phase (Figure 4E-F).

The PDX tumors treated for 10 and 28 days of vehicle control, fulvestrant and imlunestrant were subjected to RNAseq analysis. Differential gene expression comparing treatment with vehicle control and imlunestrant or fulvestrant revealed a higher number of significant changes with imlunestrant versus fulvestrant treatment on day 10 and day 28 (Figure 5A and Supplemental Table 3). In addition, K-medoids (KM) clustering of the RNAseq as early as day 10 and after 28 days detected two main gene

clusters that segregated the tumors treated with imlunestrant from fulvestrant and vehicle control, highlighting the differences between these two ER antagonists in vivo (Figure 5B-C). Pathway analysis showed that overall imlunestrant and fulvestrant impacted similar pathways, such as the downregulation of pathways related to estrogen response and the cell cycle. Additionally, there were a number of pathways that were uniquely modulated by imlunestrant, as an example the upregulation of NFKB signaling and interferon-gamma response, a pathway that was reported to be regulated by ET (21), was observed only with imlunestrant in this model. However, direct comparison of the tumors after imlunestrant and fulvestrant treatments at both time points showed that imlunestrant had more robust effects on cell cycle, estrogen response late and MYC targets pathways (Figure 5D). Taken together, these results demonstrate that in vivo better ER targeting with imlunestrant results in superior cell cycle suppression and enhanced tumor regression.

Molecular docking in the presence of the Y537S mutant ligand binding domain reveals differences between imlunestrant and fulvestrant

SERDs classically function by competitively binding to the ER ligand binding domain orthosteric hormone binding pocket. This action favors helix 12 binding within the activating function 2 (AF-2) cleft, blocking coactivator binding and increasing the dynamics of this region to promote proteasomal degradation of the receptor (22). Since imlunestrant exhibited superior Y537S *ESR1* mutant protein degradation and enhanced suppression of tumor growth in the Y537S *ESR1* mutant PDX model-compared to fulvestrant, even with a fulvestrant dose that is considered above the clinically relevant therapeutic range (23), we hypothesized that imlunestrant impacts helix 12 differently than fulvestrant.

Due to our inability to obtain diffraction quality crystals to understand the structural-basis of imlunestrant's and fulvestrant's activities, we employed molecular docking to Y537S ER ligand binding domain to test this hypothesis. At the most favorable binding energies, imlunestrant is predicted to occupy the orthosteric hormone binding pocket of ERα LBD Y537S. Interestingly, a bifurcated E353 and R394 hydrogen bond is predicted like other SERDs, however it was not predicted to bind D351 (Figure 5E).

We then sought to compare this predicted structure to that of fulvestrant. However, no co-crystal structure has been published to date. To address this, we aligned imlunestrant with a desmethyl derivative of ICI 164,384 that is an estradiol derivative chemically similar to fulvestrant (PDB: 7R62) (24). In this case, the aliphatic ICI molecule appears to directly perturb helix 12, while imlunestrant is predicted to mobilize the preceding loop. This destabilization of the loop that connects helix 11 to helix 12 has been previously shown to be sufficient to induce proteasomal degradation of the receptor (22, 25) (Figure 5F). Taken together, these data suggest that imlunestrant is likely to target the Y537S mutant ER ligand binding domain structural features that are different from fulvestrant.

Genome wide CRISPR screen to detect potential novel therapeutics in combination with imlunestrant

We performed a genome-wide CRISPR/Cas9-knockout screen with the following aims: to further test the on-target effects of imlunestrant and to identify acquired vulnerabilities in the presence of imlunestrant that are putative therapeutic targets in combination with imlunestrant that could potentiate the activity of a single agent SERD. Cells induced with the genome wide CRISPR-cas9 library were treated with DMSO or imlunestrant and collected on days 0, 14, and 31 (10 cell doublings), followed by the analysis of gRNA positive or negative selection using the Mageck algorithm (26) (Figure 6A).

Essentiality was determined based on the day 31 results and we included the results of day 14 to illustrate the kinetics of the screen (Supplemental Table 4). As expected, we detected positive enrichment of gRNAs targeting tumor suppressors, PTEN, TSC1 and TSC2, in both DMSO and imlunestrant treated cells on days 14 and day 31, indicating that loss of PTEN and TSC1/2- enhance tumor cell growth without and with imlunestrant treatment (Figure 6B-E). Conversely, we found that the essentiality score (beta-score) of several genes with key functions in HR+ breast cancer was different after imlunestrant treatment and DMSO control conditions (both compared to day 0). The *ESR1* gene was not significantly essential after 31 days of imlunestrant treatment (Beta score -0.88), whereas in cells treated with DMSO for 31 days ESR1 was essential (Beta score =-2.05) (Figure 6E). This result suggests that with long-term treatment with imlunestrant, ER is not essential providing a signal of adaptation to the treatment and supporting the on-target activity of imlunestrant. Interestingly, after 31 days of treatment with imlunestrant or DMSO, the essentiality score of *FOXA1* increased, whereas the essentiality score of *GATA3* increased only after imlunestrant treatment (Figure 6F). These different dynamics in the essentiality scores highlight the unique functions of these lineage-defining transcription factors. Genes related to the cyclin D1-Rb1 axis, such as *CCND1, CDK4* and *CDK2* were among the most essential genes in DMSO treated cells. These genes remained essential after imlunestrant treatment, albeit had lower essentiality scores when compared to DMSO treatment. Notably, CDK7, a master regulator of the cell cycle and transcription, and a dependency in ER-Y537S cells and CDK4/6i resistance (14, 19), was essential with imlunestrant treatment (Figure 6G). In addition, a number of genes that were essential in DMSO treated cells that can be targeted by drugs that are approved for the treatment of HR+ breast cancer retained essentiality after imlunestrant treatment, such as *PIK3CA*, *MTOR1* and *AKT1* (27-29) (Figure 6H). In summary, these results validate our CRISPR screening approach, highlight the on-target activity of imlunestrant and offer potential therapeutic combinations to enhance the activity of imlunestrant.

We next compared the essentiality scores (beta-score) of the CRISPR screens after 31 days of DMSO control and imlunestrant (Figure 7A). This comparison identified a set of genes that gained essentiality only after imlunestrant treatment (lower beta-scores) or decreased dependency (higher beta-scores). Pathway analysis revealed that the genes with gained essentiality are involved in pathways that are known to be associated with resistance to endocrine therapy, such as MTOR1 signaling, MYC targets (3, 30) (Figure 7B). Interestingly, multiple genes related to reactive oxygen species (ROS) and oxidative phosphorylation pathway (OXPHOS) were among the top ranked genes that gained essentiality after 31 days of imlunestrant treatment (Figure 7B-C). The OXPHOS metabolic pathway enables the production of ATP by the transport of electrons through a series of transmembrane protein complexes in the mitochondrial membrane. ROS are byproducts of the OXPHOS pathway and therefore these pathways are highly connected. Several cancers were shown to be reliant on OXPHOS and upregulation of OXPHOS was shown to be a mechanism of drug resistance in several cancers (31, 32). Specifically, the genes with the most significant beta score in these pathways that also gained essentiality after imlunestrant treatment included SOD1, NDUFSA3, NDUFC1and NDUFS2 (Figure 7C). These genes are critical components of mitochondrial energy metabolism and cellular redox balance. SOD1 is a Cu/Zn superoxide dismutase that plays a major role in redox balance and protects against superoxide radicals (33). NDUFA3 (NADH:ubiquinone oxidoreductase subunit A3 and C1) is predicted to be involved in assembly of complex I in the mitochondrial OXPHOS respiratory chain, and NDUFC1 and NDUFS2 are complex I core components. Taken together, these genes are key components of redox balance and mitochondria OXPHOS and these results provide a rationale for testing inhibitors of these pathways, particularly inhibitors of the OXPHOS complex 1, in combination with imlunestrant.

To follow-up on our CRISPR screen results and test the effect of pharmacological inhibition of OXPHOS we used the small molecule inhibitor of OXPHOS complex I, IACS-010759 (IACS) (34). We did not observe a substantial effect on growth after 9 days of treatment with IACS alone at a concentration of 10 nM or when IACS was added to imlunestrant in MCF7 cells (Figure 7D). In contrast, in T47D cells, IACS alone suppressed cell growth and there was a small added effect when combined with imlunestrant. In the MCF7 and T47D endocrine resistant cells expressing the Y537S *ESR1* mutation we observed a dose response effect with IACS in both MCF7 and T47D cells, and again with superior activity in the T47D cells (Figure 7E). Importantly, there was significant synergy between IACS and imlunestrant in the MCF7 cells expressing the Y537S mutation (Figure 7F). Finally, imlunestrant-resistant cells were generated by culturing MCF7 in the presence of escalating doses of imlunestrant. As expected, imlunestrant-resistant cells displayed an increased IC50 and increased confluency of colonies after imlunestrant treatment (Figure 7G-I). While IACS alone already resulted in a significant decrease in the colony confluency in the imlunestrant-resistance cells, the addition of imlunestrant to IACS enhanced this effect (Figure 7H-I). In aggregate, these results provide evidence for the tumor suppressive effect of OXPHOS complex I inhibition in combination with imlunestrant as a potential strategy to enhance the activity of imlunestrant and overcome resistance to imlunestrant in ER+ breast cancer.

Discussion

SERDs have several potential advantages compared to SERMS and aromatase inhibitors. Specifically, the pure antagonistic activity of SERDs that precedes the increase in the turnover of ER is a key feature that differentiates this class of drugs from SERMS, which have context dependent agonistic activity in addition to their antagonistic activity (35). In addition, the ability of SERDS to

enhance ER degradation can potentially circumvent ligand independent activity, a key mechanism of endocrine resistance in which ER remains a key tumor driver.

Fulvestrant, the first-in-class SERD, is limited by its poor bioavailability requiring intra-muscular injections and poor pharmacokinetics. The CONFIRM clinical trial showed that a higher dose of fulvestrant (500mg versus 250mg) resulted in superior clinical outcomes (36, 37), but FES-PET imaging indicated incomplete ER antagonism with fulvestrant treatment even at the higher doses (38). More recently, retrospective analyses of clinical trials indicate that the presence of the LBD activating ER mutations confer resistance to fulvestrant (12). Taken together, these limitations of fulvestrant provide a rationale for developing next-generation oral SERDs with improved pharmacokinetics and activity against the *ESR1* mutations.

Imlunestrant is an oral SERD in clinical development. Pre-clinical studies also demonstrated that imlunestrant is brain penetrant (39). The phase I/1b EMBER study (NCT04188548) investigating imlunestrant as a single agent and in combination with other targeted agents, established the recommended phase 2 dose (RP2D) of imlunestrant (18). The phase III EMBER 3 clinical trial investigated imlunestrant versus fulvestrant versus imlunestrant plus abemacilib in patients with advanced ER+ breast cancer who have progressed on first line endocrine therapy-based treatment and showed that imlunestrant had superior activity compared to fulvestrant in patients with an *ESR1* mutation (40). The phase III EMBER 4 clinical trial (NCT05514054) is investigating adjuvant imlunestrant versus standard of care endocrine therapy after 2 years and within 5 years of adjuvant treatment. In addition to imlunestrant, there are several other next generation oral endocrine therapies that are either already approved (elacestrant) or are in advanced phases of clinical development

(camizestrant, vepdegestrant and giredestrant) (17). We did not investigate how these other agents compare to imlunestrant, which is a limitation of our study.

In this study, we investigated the pre-clinical pharmacology and efficacy of imlunestrant in WT and hormone-resistant mutant ER and demonstrated several clinically relevant characteristics of imlunestrant. Our studies focused on the Y537S ER mutation since it has been shown to have the most robust phenotypes, including both its constitutive and antagonistic activity[14]. Imlunestrant exhibited pure antagonistic activity preceding the degradation activity. In addition, imlunestrant leads to ER degradation in the presence of WT and mutant ER. Compared to fulvestrant, imlunestrant demonstrated superior degradation of the Y537S mutant ER, which could potentially be explained by the differences in the molecular docking of these two agents in the presence of the mutant ligand binding domain. Remarkably, we demonstrate the highly specific on-target activity of imlunestrant, as evidenced by the absence of gene expression changes when treating cells in which ER transcriptional activity was suppressed by hormone deprivation.

In the in vitro studies we did not observe superior tumor cell growth suppression with imlunestrant compared to fulvestrant in the presence of the Y537S ER mutation. However, our in vivo study in a PDX model harboring a Y537S mutation demonstrates that improved ER blockade with imlunstrant led to enhanced tumor suppression with evidence of tumor regression, despite resistance to a relatively high dose of fulvestrant that is considered above the clinically relevant therapeutic dose (23). Molecular analysis of the tumors at early points showed enhanced ER degradation with imlunestrant versus fulvestrant. Importantly, comprehensive analysis of the cell cycle using Ki67, the MPI algorithm and transcriptomic data, provides evidence that in the presence of an *ESR1* mutation, better ER targeting is associated with increased cell cycle inhibition and potentiates tumor growth

suppression. In addition, transcriptomic analysis showed that imlunestrant treatment resulted in increased expression of interferon gamma response and NFKB signaling, consistent with a previous study showing that ER blockade induces increased Rel A chromatin binding and NFKB signaling, which in turn increases the expression of genes involved in the interferon gamma pathway in a cell intrinsic manner (21). This may have important therapeutic implications and warrants further pre-clinical investigation of the combination of SMAC mimetics (21), immune therapies and imlunestrant in HR+ breast cancer models.

Our genome wide CRISPR knock-out screen during imlunestrant treatment showed that known vulnerabilities in HR+ breast, such as genes related to the CDK4/6-RB1 axis and PI3Kinase signaling pathway, remain essential in the presence of imlunestrant treatment. This supports the clinical investigation of imlunestrant in combination with drugs targeting these pathways, such as CDK4/6i and PI3Kinase and AKT inhibitors. In addition, we identified a new vulnerability that is a potential therapeutic target. Several genes related to OXPHOS were among the top genes that gained essentiality during imlunestrant treatment. As a follow up of these results, we showed synergistic activity between imlunestrant and the OXPHOS inhibitor IACS in cells expressing the ER Y537S mutation. In addition, cells with acquired resistance to imlunestrant were sensitive to IACS. These results are in line with studies showing that in more aggressive cancers, treatment resistance or metastases there is a switch from aerobic glycolysis to OXPHOS for ATP generation (41). Moreover, recent studies also showed that with the acquisition of endocrine resistance there is a metabolic rewiring characterized by the dependency on OXPHOS (42, 43). Disappointingly, the phase I clinical trial of IACS failed to establish the recommended RP2D because of dose limiting toxicities (44). However, this study investigated IACS as a single agent and it is possible that the addition of a low dose of IACS would be tolerated and could be utilized to enhance the activity of imlunestrant and

prolong disease control. Nevertheless, these results unveil a key metabolic compensatory mechanism of resistance to imlunestrant and supports further investigation of approaches to target this metabolic change for therapeutic purposes. We also identified CDK7 as one of the top ranked vulnerabilities during imlunestrant treatment. In keeping with this finding, in previous studies we identified CDK7 as a potential therapeutic target in ER+ breast cancer and selective CDK7 inhibitors are currently in clinical development in metastatic HR+ breast cancer (45).

In summary, we provide pre-clinical evidence of imlunestrant's selective on-target antagonistic activity. Importantly, imlunestrant as a single agent can overcome resistance engendered by the Y537S *ESR1* mutation. In addition, we identified several genes that gained essentiality during treatment with imlunestrant that can be targeted pharmacologically, offering a rational for clinical testing of drug combinations, such as CDK4i, CDK7i, PI3Kinase inhibitors with imlunestrant.

Materials and Methods

Sex as a biological variable

Our study exclusively examined female mice because the disease modeled is mostly relevant in females, male breast cancer is rare.

Cell lines

Cell lines were purchased from ATCC, independently validated using SPR testing, and routinely tested for mycoplasma contamination. Cells were maintained in sterile culture at 37 degrees C and 5% CO2. MCF7 cells were grown in DMEM supplemented with 10% FBS, 1X Penicillin/Streptomycin, and 10 ug/mL recombinant human insulin. T47D cells were grown in RPMI supplemented 10% FBS, 1X

Penicillin/Streptomycin, and 1% glutamine. HEK293T cells were grown in DMEM supplemented with 10% FBS, 1X Penicillin/Streptomycin, 1X sodium pyruvate, 1X non-essential amino acids, and 1X glutamine. As indicated, cells were hormone deprived (HD) for 72 hours by media change into phenol red free media supplemented with 10% charcoal dextran treated FBS. MCF7 cells with a doxycycline-inducible Y537S mutation (MCF7-Y537S) in ER *and* T47D cells with a doxycycline-inducible Y537S mutation (T47D-Y537S) were created as previously described (14). For doxycycline-inducible expression of ER-Y537S cells were treated with 1ug/mL doxycycline for 48-72 hours. To generate imlunestrant-resistant cells, MCF7 cells were cultured in increasing concentrations of imlunestrant (i.e long term exposure [LTE]) starting from 1nM and ending at 100nM. Imlunestrant was provided by Lilly for most of the experiments except for the experiments in Figures 7D-I. For these experiments imlunestrant was purchased from MedChem Express (HY-145572).

ERE-LUC

MCF7 cells stably expressing a luminescent reported under control of an estrogen response element (MCF7 ERE-LUC) were used to measure agonistic activity of ER ligands (46). Cells (1x10^3) were plated in each well of a white opaque 96 well plate in at least quadruplicate. The next day media was change to HD media supplemented with the indicated treatment. After treatment, luminescence was measured using a microplate reader. For normalization, protein content was measured by addition of BCA reagent and colorimetric measurement using a microplate reader.

Western blot

Cells ($2x10^6$) were plated in a 10cm2 dish. The next day, the media was changed to HD media with or without doxycycline. Cells were treated as indicated for 24 hours followed by cell lysis in RIPA buffer

supplemented with protease and phosphatase inhibitors. Protein concentrations were normalized using BCA assay, SDS-PAGE was performed using the BioRad mini electrophoresis system and 4-12% NuPage Bis/Tris gels, proteins were transferred to nitrocellulose membranes using a BioRad mini Turbo, and blotted for estrogen receptor (CST, #D6R2W) or GAPDH (CST #14C10). Chemiluminescence was captured using a BioRad ChemiDoc and densitometry quantification was performed on digital images in Fiji/ImageJ.

Cell proliferation

Cells (5x103) were plated in each well of a 24 well plate in full media in quadruplicate. The next day, the media was changed to include the indicated treatment. After 5 days of treatment, cells were stained using X hoescht and X propidium iodide, followed by counting the live cell number (hoescht positive and propidium iodide negative) using Celigo automated imaging platformm . Replicates were averaged and normalized to DMSO control.

Colony growth

Cells (5x10^3) were plated in each well of a 6 well plate in full media in duplicate. The next day, the media was changes to include the indicated treatment. After two weeks of treatment, cells were fixed in ice-cold methanol, stained using 0.1% crystal violet in methanol, washed in water, and dried overnight. Images were captured using a digital scanner and crystal violet area quantified using Fiji/ImageJ.

RNAseq

MCF7 or T47D cells (2x106) were plated in 10cm2 dishes in triplicate. The next day, media was changed to HD media with or without doxycycline. Cells were treated with estradiol (10nM), imlunestrant (100nM), fulvestrant (100nM) or DMSO for 24 hours. Cells were washed, snap frozen in liquid nitrogen, and RNA was extracted using Trizol and RNeasy mini (Qiagen). RNAseq was performed on the NovaSeqX platform. The VIPER pipeline was used for the alignment and quality control (47) of the samples. Alignment to the hg19 human genome was done with STAR v2.7.0 (48) and transcript assembly was done with cufflinks v2.2.1 (49). Quality control was done with RseQC v2.6.2 (50, 51).We assessed each sample on metrics of mappable reads, percentage of rRNA reads, gene body coverage, junction saturation and insert size for paired ends, and exploratory data analysis on variance-stabilized counts to determine samples that were of adequate quality. Differential expression testing was done using DESeq2 v1.44.0 (52) and ashr_v2.2-63 (53). Genes plotted in expression heatmaps were clustered by partitioning around medoids using the cluster v2.1.8 R package (https://CRAN.R-project.org/package=cluster). Genes were considered significantly differentially expressed if their ashr-shrunken log2 fold change was ≥ 1 with an adjusted P-value < 0.10. Gene set testing on the Hallmark gene collection (54) was performed using the pre-ranked version of correlation adjusted mean rank gene set test (cameraPR) using limma v3.60.6 (55, 56), where genes were pre-ranked by their Wald statistics from DESeq2 testing. Multiple testing was accounted for using the Benjamini-Hochberg procedure by controlling at a 10% false discovery rate (FDR). Analyses were performed using R v4.4.1 [R Core Team (2024). _R: A Language and Environment for Statistical Computing_. R Foundation for Statistical Computing, Vienna, Austria. <https://www.R-project.org/>.]

Animal studies

All mice were maintained in accordance with local guidelines and therapeutic interventions approved by the Animal Care and Use Committees of Dana-Farber Cancer Institute. These patient-derived xenograft (PDX) details were published previously (57). Tumor fragments from the Y537S ER-mutant PDX1526 were dipped in 50% matrigel and implanted into the fourth mammary fat pads of ovariectomized NOD-SCID-IL2Rgc–/– mice (Jackson Laboratories) without estradiol (E2) supplements. Anesthesia for the implantation was performed with isoflurane mixed with medical air. When tumors reached 150–200 mm3, mice were randomized into 3 groups ($N = 5–8$ mice per group): vehicle control (DMSO), fulvestrant 5 mg sc/week subcutaneous, imlunestrant 15mg/kg daily oral gavage for 28 days. Tumor volumes were measured at least once a week. Additional 3 mice per group were treated for 10 days only. After treatment mice were euthanized, and tumors were harvested. Mouse euthanasia was performed using carbon dioxide (CO2), followed by cervical dislocation. Tumors were halved for snap freezing frozen for RNA extraction and the other half for fixing in formalin and paraffin embedding for immunohistochemistry and immunofluorescence staining.

Immunohistochemistry

Immunohistochemistry was performed on the Leica Bond III automated staining platform using the Leica Biosystems Refine Detection Kit (Leica; DS9800). FFPE tissue sections were baked for 30 minutes at 60°C and deparaffinized (Leica AR9222) prior to staining. Primary antibodies were incubated for 30 minutes, visualized via DAB, and counterstained with hematoxylin (Leica DS9800). The slides were rehydrated in graded alcohol and coverslipped using the HistoreCore Spectra CV mounting medium (Leica 3801733). The slides were stained with the following antibodies: Ki67 from Biocare Medical, catalog number PRM325, clone SP6 was run at the ready to use concentration with a 20M EDTA antigen retrieval (Leica ER2 AR9640), Progesterone Receptor from Dako, catalog number

M3569, clone PgR 636 was run at 1:400 dilution with a 20M EDTA antigen retrieval (Leica ER2 AR9640) and ER alpha from Neomarkers, catalog number RM-9101, clone SP1 was run at 1:40 dilution with a 30M citrate antigen retrieval (Leica ER2 AR9961).

CyCIF MPI

The methods for CycIF and MPI calculation were previously described[20]. Briefly, FFPE slides were baked at 60°C for 30 minutes, dewaxed using Bond Dewax solution at 72°C, and antigen retrieval was performed with Epitope Retrieval 1 solution at 100°C for 20 minutes using the BOND RX Automated IHC/ISH Stainer. Antibodies for each cycle were diluted in Odyssey Blocking Buffer and incubated overnight at 4°C in the dark. After antibody incubation, slides were stained with Hoechst 33342 for 10 minutes at room temperature. Slides were cover slipped using 20–50% glycerol solution (Sigma, G5516) in PBS. Images were taken using DAPI, FITC, Cy3, and Cy5 channels either on the RareCyte CyteFinder (20x/0.75NA objective). After imaging, fluorophores were inactivated (4.5% H2O2, 20mM NaOH in PBS, 45 minutes) under LED lights, and the next cycle was performed. CyCIF image processing is organized in the following steps: Stitching, registration, correction of acquisition artifacts was performed using ASHLAR and the BaSiC algorithm. Ilastik software was trained on cropped images to label nuclear, cytoplasmic, and background areas. Pan-cytokeratin positivity was used as the threshold for determining epithelial cells, which are the cells which were included in the analysis. Data aggregation, filtering, normalization and analysis were performed as previously described (20). Multivariate Proliferation Index (MPI) calculation; MPI is based on the normalized measurement of 5 markers: three proliferation markers (Ki-67 [CST #11882S], MCM2 [Abcam 223403], PCNA [CST# 8580S) and two cell cycle arrest markers (p21[CST 8493s], p27[ab206927]). The method avoids relying on single markers while separating cells expressing high level arrest markers (even if

proliferation markers are expressed). The threshold values for proliferation and arrest are dataset dependent. Additional details and access to the underlying code can be found at https://github.com/labsyspharm/ashlar and https://github.com/santagatalab.

CRISPR screen

The H3 genome wide gRNA library (Addgene #133914) (this library targets more than 18,000 annotated genes in the human genome, with 6 gRNAs per gene on average for a total of 117,587 gRNAs and 3,842 gRNAs targeting controls AAVS1, ROSA26 and CCR5) in the pLentiCRISPRv2 backbone was co-transfected with the packaging plasmids, pSPAX and pMD2G, into HEK293T cells using OptiMem and Xtreme gene transfection reagent according to manufacturer's instructions. After 72 hours the lentiviral supernatant was collected, cleared by centrifugation and syringe filter, followed by freezing aliquots at -80 degrees C. For the CRISPR screen, T47D cells (2.7x108) were transduced in suspension with 100 ug/mL polybrene at MOI = 0.3. Cells were selected in 1.5 ug/mL puromycin for 96 hours, cells were passaged, 3x106 cells were collected for the day 0 sample, or 3x106 cells were plated for DMSO or imlunestrant treatment. Cells were maintained in full growth media with 1nM of imlunestrant or DMSO for 14 or 31 days. Cells were collected, washed, snap frozen in liquid nitrogen, and stored at -80 degrees C. DNA was extracted using DNAeasy kit (Qiagen), gRNA barcodes were PCR amplified with adapters for sequencing on the Illumina platform. DNA libraries were sequenced at the DFCI Molecular biology core facility using the NextSeq5000 system. Sequencing results were analyzed using MAGeCK-VISPR (26) and MAGeCK-FLUTE v2.8.0 (R package version 2.8.0, <https://bioconductor.org/packages/MAGeCKFlute>).

BLISS synergy assay

MCF7 cells in full growth media were treated with doxycycline for 48 hours, then cells (1x103) were seeded in each well of a 96 well plate at least in quadruplicate. The next day, cells were treated as indicated with imlunestrant, IACS, or DMSO. Cells were treated with an eight-point dose response matrix using three-fold steps centered around each drug IC50. After treatment for five days, live cell number was counted using Celigo, and synergy quantified using BLISS synergy tool (https://synergyfinder.fimm.fi/synergy/20240901234814724196/).

Molecular docking modeling

Protein x-ray crystal structures were retrieved from RCSB PDB. Python Molecular Viewer was used to add polar hydrogens and Kollman Charges before docking the ligand over the ligand binding pocket using AutoDock Vina. Results were visualized using PyMOL.

Statistics

Statistical analysis was performed in Prism 3.0 (Graphpad). Student's t-test was performed when comparing two groups and ANOVA test was performed for multiple comparisons. P-values < 0.05 are considered significant and the corresponding statistical tests are reported in the figure legends.

Study approval

For PDX studies, patient consent for tumor implantation in nude mice was obtained under an IRB approved protocol (Dana-Farber/Harvard Cancer Center IRB protocol 93-085) and with patient consent and in compliance with the Declaration of Helsinki.

Data availability

RNAseq data has been deposited to GEO database with the accession number GSE295024. All data values for all graphs are included in the supporting data values file.

Acknowledgements

This work was conducted with support from Lilly, NIH NCI R01CA237414 (to RJ) the Maor Foundation (to RJ), The Kroesser Family Fund (to RJ), The Melanie Rosay Fund (to RJ), Steven Koster Fund (to RJ), and NIH NCI R37CA279341 (to SWF). The authors thank Dr. Myles Brown (Department of Medical Oncology, Dana-Farber Cancer Institute, Boston, MA, USA) for his insightful comments. We thank Dana-Farber/Harvard Cancer Center in Boston, MA, for the use of the Specialized Histopathology Core, which provided histology and immunohistochemistry service. Dana-Farber/Harvard Cancer Center is supported in part by an NCI Cancer Center Support Grant # NIH 5 P30 CA06516.

Author contributions

SS (Shira Sherman), ZS, SF, and RJ conceptualized the study and wrote the manuscript. SS (Shira Sherman), DR, AV, DZ, GG, SK, and GK conducted the formal analysis. RJ acquired funding for the study. SS (Shira Sherman), ZS, AN, CH, DF, GK, AV, and FHP completed the experiments and data collection. QDN, SS (Sandro Santagata), SF, and RJ supervised the study. ZS, DR, and AV prepared the figures for publication. All authors reviewed and edited the manuscript and approved the final manuscript.

Competing Interests

RJ declares research funds from Pfizer, Lilly and Novartis, and advisory/consultant role for Lilly, Pfizer, GE Health, Carrick Therapeutics, Luminex and Novartis. AN is currently an employee at AstraZeneca. GG is currently an employee at Sanofi.

References

1. Carroll JS, Liu XS, Brodsky AS, Li W, Meyer CA, Szary AJ, et al. Chromosome-wide mapping of estrogen receptor binding reveals long-range regulation requiring the forkhead protein FoxA1. Cell. 2005;122(1):33-43.
2. Shao W, Keeton EK, McDonnell DP, and Brown M. Coactivator AIB1 links estrogen receptor transcriptional activity and stability. Proc Natl Acad Sci U S A. 2004;101(32):11599-604.
3. Nardone A, De Angelis C, Trivedi MV, Osborne CK, and Schiff R. The changing role of ER in endocrine resistance. Breast. 2015;24 Suppl 2(0 2):S60-6.
4. Hagio K, Baba M, Ishida N, Oshino T, Kasahara R, Nara M, et al. Tamoxifen withdrawal in women with progressive metastatic breast cancer: a case series of six patients. Int Cancer Conf J. 2018;7(4):142-7.
5. Kato S, Endoh H, Masuhiro Y, Kitamoto T, Uchiyama S, Sasaki H, et al. Activation of the estrogen receptor through phosphorylation by mitogen-activated protein kinase. Science. 1995;270(5241):1491-4.
6. Massarweh S, Osborne CK, Creighton CJ, Qin L, Tsimelzon A, Huang S, et al. Tamoxifen resistance in breast tumors is driven by growth factor receptor signaling with repression of classic estrogen receptor genomic function. Cancer Res. 2008;68(3):826-33.
7. Grinshpun A, Sandusky ZM, and Jeselsohn R. The Clinical Utility of ESR1 Mutations in Hormone Receptor-Positive, HER2-Negative Advanced Breast Cancer. Hematol Oncol Clin North Am. 2023;37(1):169-81.
8. Jeselsohn R, Yelensky R, Buchwalter G, Frampton G, Meric-Bernstam F, Gonzalez-Angulo AM, et al. Emergence of constitutively active estrogen receptor-alpha mutations in

pretreated advanced estrogen receptor-positive breast cancer. Clin Cancer Res. 2014;20(7):1757-67.

9. Hosfield DJ, Weber S, Li N-S, Sauvage M, Joiner CF, Hancock GR, et al. Stereospecific lasofoxifene derivatives reveal the interplay between estrogen receptor alpha stability and antagonistic activity in ESR1 mutant breast cancer cells. eLife. 2022;11:e72512.

10. Fanning SW, Mayne CG, Dharmarajan V, Carlson KE, Martin TA, Novick SJ, et al. Estrogen receptor alpha somatic mutations Y537S and D538G confer breast cancer endocrine resistance by stabilizing the activating function-2 binding conformation. eLife. 2016;5:e12792.

11. Katzenellenbogen JA, Mayne CG, Katzenellenbogen BS, Greene GL, and Chandarlapaty S. Structural underpinnings of oestrogen receptor mutations in endocrine therapy resistance. Nat Rev Cancer. 2018;18(6):377-88.

12. O'Leary B, Hrebien S, Morden JP, Beaney M, Fribbens C, Huang X, et al. Early circulating tumor DNA dynamics and clonal selection with palbociclib and fulvestrant for breast cancer. Nat Commun. 2018;9(1):896.

13. Fanning SW, Mayne CG, Dharmarajan V, Carlson KE, Martin TA, Novick SJ, et al. Estrogen receptor alpha somatic mutations Y537S and D538G confer breast cancer endocrine resistance by stabilizing the activating function-2 binding conformation. Elife. 2016;5.

14. Jeselsohn R, Bergholz JS, Pun M, Cornwell M, Liu W, Nardone A, et al. Allele-Specific Chromatin Recruitment and Therapeutic Vulnerabilities of ESR1 Activating Mutations. Cancer Cell. 2018;33(2):173-86 e5.

15. Bidard FC, Kaklamani VG, Neven P, Streich G, Montero AJ, Forget F, et al. Elacestrant (oral selective estrogen receptor degrader) Versus Standard Endocrine Therapy for Estrogen Receptor-Positive, Human Epidermal Growth Factor Receptor 2-Negative Advanced Breast Cancer: Results From the Randomized Phase III EMERALD Trial. J Clin Oncol. 2022;40(28):3246-56.

16. Downton T, Zhou F, Segara D, Jeselsohn R, and Lim E. Oral Selective Estrogen Receptor Degraders (SERDs) in Breast Cancer: Advances, Challenges, and Current Status. Drug Des Devel Ther. 2022;16:2933-48.

17. Corti C, De Angelis C, Bianchini G, Malorni L, Giuliano M, Hamilton E, et al. Novel endocrine therapies: What is next in estrogen receptor positive, HER2 negative breast cancer? Cancer Treat Rev. 2023;117:102569.

18. Jhaveri KL, Lim E, Jeselsohn R, Ma CX, Hamilton EP, Osborne C, et al. Imlunestrant, an Oral Selective Estrogen Receptor Degrader, as Monotherapy and in Combination With Targeted Therapy in Estrogen Receptor-Positive, Human Epidermal Growth Factor Receptor 2-Negative Advanced Breast Cancer: Phase Ia/Ib EMBER Study. J Clin Oncol. 2024:JCO2302733.

19. Guarducci C, Nardone A, Russo D, Nagy Z, Heraud C, Grinshpun A, et al. Selective CDK7 inhibition suppresses cell cycle progression and MYC signaling while enhancing apoptosis in therapy-resistant estrogen receptor positive breast cancer. Clin Cancer Res. 2024.

20. Gaglia G, Kabraji S, Rammos D, Dai Y, Verma A, Wang S, et al. Temporal and spatial topography of cell proliferation in cancer. Nat Cell Biol. 2022;24(3):316-26.

21. Hermida-Prado F, Xie Y, Sherman S, Nagy Z, Russo D, Akhshi T, et al. Endocrine Therapy Synergizes with SMAC Mimetics to Potentiate Antigen Presentation and Tumor

Regression in Hormone Receptor-Positive Breast Cancer. Cancer Res. 2023;83(19):3284-304.

22. Fanning SW, Hodges-Gallagher L, Myles DC, Sun R, Fowler CE, Plant IN, et al. Specific stereochemistry of OP-1074 disrupts estrogen receptor alpha helix 12 and confers pure antiestrogenic activity. Nat Commun. 2018;9(1):2368.

23. Wardell SE, Yllanes AP, Chao CA, Bae Y, Andreano KJ, Desautels TK, et al. Pharmacokinetic and pharmacodynamic analysis of fulvestrant in preclinical models of breast cancer to assess the importance of its estrogen receptor-alpha degrader activity in antitumor efficacy. Breast Cancer Res Treat. 2020;179(1):67-77.

24. Wakeling AE, and Bowler J. Steroidal pure antioestrogens. J Endocrinol. 1987;112(3):R7-10.

25. Fanning SW, Jeselsohn R, Dharmarajan V, Mayne CG, Karimi M, Buchwalter G, et al. The SERM/SERD bazedoxifene disrupts ESR1 helix 12 to overcome acquired hormone resistance in breast cancer cells. Elife. 2018;7.

26. Li W, Xu H, Xiao T, Cong L, Love MI, Zhang F, et al. MAGeCK enables robust identification of essential genes from genome-scale CRISPR/Cas9 knockout screens. Genome Biol. 2014;15(12):554.

27. Baselga J, Campone M, Piccart M, Burris HA, 3rd, Rugo HS, Sahmoud T, et al. Everolimus in postmenopausal hormone-receptor-positive advanced breast cancer. N Engl J Med. 2012;366(6):520-9.

28. Andre F, Ciruelos E, Rubovszky G, Campone M, Loibl S, Rugo HS, et al. Alpelisib for PIK3CA-Mutated, Hormone Receptor-Positive Advanced Breast Cancer. N Engl J Med. 2019;380(20):1929-40.

29. Turner NC, Oliveira M, Howell SJ, Dalenc F, Cortes J, Gomez Moreno HL, et al. Capivasertib in Hormone Receptor-Positive Advanced Breast Cancer. N Engl J Med. 2023;388(22):2058-70.

30. Musgrove EA, and Sutherland RL. Biological determinants of endocrine resistance in breast cancer. Nat Rev Cancer. 2009;9(9):631-43.

31. Xu Y, Xue D, Bankhead A, 3rd, and Neamati N. Why All the Fuss about Oxidative Phosphorylation (OXPHOS)? J Med Chem. 2020;63(23):14276-307.

32. Sica V, Bravo-San Pedro JM, Stoll G, and Kroemer G. Oxidative phosphorylation as a potential therapeutic target for cancer therapy. Int J Cancer. 2020;146(1):10-7.

33. Kumari S, Badana AK, G MM, G S, and Malla R. Reactive Oxygen Species: A Key Constituent in Cancer Survival. Biomark Insights. 2018;13:1177271918755391.

34. Molina JR, Sun Y, Protopopova M, Gera S, Bandi M, Bristow C, et al. An inhibitor of oxidative phosphorylation exploits cancer vulnerability. Nat Med. 2018;24(7):1036-46.

35. Hodges LC, Cook JD, Lobenhofer EK, Li L, Bennett L, Bushel PR, et al. Tamoxifen functions as a molecular agonist inducing cell cycle-associated genes in breast cancer cells. Mol Cancer Res. 2003;1(4):300-11.

36. Di Leo A, Jerusalem G, Petruzelka L, Torres R, Bondarenko IN, Khasanov R, et al. Results of the CONFIRM phase III trial comparing fulvestrant 250 mg with fulvestrant 500 mg in postmenopausal women with estrogen receptor-positive advanced breast cancer. J Clin Oncol. 2010;28(30):4594-600.

37. Shang Y, and Brown M. Molecular determinants for the tissue specificity of SERMs. Science. 2002;295(5564):2465-8.

38. van Kruchten M, de Vries EG, Glaudemans AW, van Lanschot MC, van Faassen M, Kema IP, et al. Measuring residual estrogen receptor availability during fulvestrant therapy in patients with metastatic breast cancer. Cancer Discov. 2015;5(1):72-81.

39. Bhagwat SV, Mur C, Vandekopple M, Zhao B, Shen W, Marugan C, et al. Imlunestrant Is an Oral, Brain-Penetrant Selective Estrogen Receptor Degrader with Potent Antitumor Activity in ESR1 Wild-Type and Mutant Breast Cancer. Cancer Res. 2025;85(4):777-90.

40. Jhaveri KL, Neven P, Casalnuovo ML, Kim SB, Tokunaga E, Aftimos P, et al. Imlunestrant with or without Abemaciclib in Advanced Breast Cancer. N Engl J Med. 2025;392(12):1189-202.

41. Jia D, Park JH, Jung KH, Levine H, and Kaipparettu BA. Elucidating the Metabolic Plasticity of Cancer: Mitochondrial Reprogramming and Hybrid Metabolic States. Cells. 2018;7(3).

42. El-Botty R, Morriset L, Montaudon E, Tariq Z, Schnitzler A, Bacci M, et al. Oxidative phosphorylation is a metabolic vulnerability of endocrine therapy and palbociclib resistant metastatic breast cancers. Nat Commun. 2023;14(1):4221.

43. Navarro-Yepes J, Kettner NM, Rao X, Bishop CS, Bui TN, Wingate HF, et al. Abemaciclib Is Effective in Palbociclib-Resistant Hormone Receptor-Positive Metastatic Breast Cancers. Cancer Res. 2023;83(19):3264-83.

44. Yap TA, Daver N, Mahendra M, Zhang J, Kamiya-Matsuoka C, Meric-Bernstam F, et al. Complex I inhibitor of oxidative phosphorylation in advanced solid tumors and acute myeloid leukemia: phase I trials. Nat Med. 2023;29(1):115-26.

45. Coombes RC, Howell S, Lord SR, Kenny L, Mansi J, Mitri Z, et al. Dose escalation and expansion cohorts in patients with advanced breast cancer in a Phase I study of the CDK7-inhibitor samuraciclib. Nat Commun. 2023;14(1):4444.

46. Gagne D, Balaguer P, Demirpence E, Chabret C, Trousse F, Nicolas JC, et al. Stable luciferase transfected cells for studying steroid receptor biological activity. J Biolumin Chemilumin. 1994;9(3):201-9.

47. Cornwell M, Vangala M, Taing L, Herbert Z, Koster J, Li B, et al. VIPER: Visualization Pipeline for RNA-seq, a Snakemake workflow for efficient and complete RNA-seq analysis. BMC Bioinformatics. 2018;19(1):135.

48. Dobin A, Davis CA, Schlesinger F, Drenkow J, Zaleski C, Jha S, et al. STAR: ultrafast universal RNA-seq aligner. Bioinformatics. 2013;29(1):15-21.

49. Trapnell C, Williams BA, Pertea G, Mortazavi A, Kwan G, van Baren MJ, et al. Transcript assembly and quantification by RNA-Seq reveals unannotated transcripts and isoform switching during cell differentiation. Nat Biotechnol. 2010;28(5):511-5.

50. Wang L, Wang S, and Li W. RSeQC: quality control of RNA-seq experiments. Bioinformatics. 2012;28(16):2184-5.

51. Wang L, Nie J, Sicotte H, Li Y, Eckel-Passow JE, Dasari S, et al. Measure transcript integrity using RNA-seq data. BMC Bioinformatics. 2016;17:58.

52. Love MI, Huber W, and Anders S. Moderated estimation of fold change and dispersion for RNA-seq data with DESeq2. Genome Biol. 2014;15(12):550.

53. Carbonetto P, Luo K, Sarkar A, Hung A, Tayeb K, Pott S, et al. GoM DE: interpreting structure in sequence count data with differential expression analysis allowing for grades of membership. Genome Biol. 2023;24(1):236.

54. Liberzon A, Birger C, Thorvaldsdottir H, Ghandi M, Mesirov JP, and Tamayo P. The Molecular Signatures Database (MSigDB) hallmark gene set collection. Cell Syst. 2015;1(6):417-25.

55. Wu D, and Smyth GK. Camera: a competitive gene set test accounting for inter-gene correlation. Nucleic Acids Res. 2012;40(17):e133.

56. Ritchie ME, Phipson B, Wu D, Hu Y, Law CW, Shi W, et al. limma powers differential expression analyses for RNA-sequencing and microarray studies. Nucleic Acids Res. 2015;43(7):e47.

57. Guarducci C, Nardone A, Russo D, Nagy Z, Heraud C, Grinshpun A, et al. Selective CDK7 Inhibition Suppresses Cell Cycle Progression and MYC Signaling While Enhancing Apoptosis in Therapy-resistant Estrogen Receptor-positive Breast Cancer. Clin Cancer Res. 2024;30(9):1889-905.

Figure Legends:

Figure 1: Antagonistic and ER degradation activity of imlunestrant

A) Cell growth studies depicted as cell number fold change for MCF7 (left) or T47D (right) cells during treatment up to 8 days with DMSO or imlunestrant (IML). Error bars denote ± standard deviation. Two-way ANOVA with Dunnett's multiple comparisons test. **B)** Normalized cell proliferation for MCF7 (left) or T47D (right) cells expressing ER wildtype or ER-Y537S and treated with a dose-response of imlunestrant for 5 days. Error bars with average ± standard deviation. Two-way ANOVA with Sidak's multiple comparisons test. **C)** Normalized luciferase signal in MCF7 ERE-LUC cells after hormone deprivation (HD) and treatment with or without E_2 (1nM) and imlunestrant (0, 50 nM, 500 nM, or 1000 nM) for 1 hr, **D)** 6 hr, or **E)** 24 hr. Bar graph with averages. Error bars denote ± standard deviation. Two-way ANOVA with Tukey's multiple comparisons test. **F)** Western blot of whole cell lysates for ER and GAPDH in MCF7 cells in HD media treated with fulvestrant (FULV; 100 nM, 24 hr) or imlunestrant (IML; 100 nM from 0 to 72 hr), as indicated. Densitometry of ER levels normalized to DMSO and GAPDH. **G)** Western blot for ER wildtype (lower band) and ER mutant (HA-tagged, upper band) and GAPDH in MCF7 ER-Y537S cells in HD media treated with FULV (100 nM, 24 hr) or IML (100 nM, 0 to 72 hr), as indicated. Densitometry of ER mutant levels normalized to DMSO and GAPDH. **H)** Colony assay crystal violet staining results from MCF7 or T47D cells with ER wildtype or ER-Y537S expression and treatment with imlunestrant (0 to 100 nM, as indicated) for two weeks in full media. **I)** Relative confluency of colony assay crystal violet staining in H). Bar graph with average ± standard deviation. One way ANOVA with Dunnett's multiple comparisons test. *p<0.05, **p<0.01, ***p<0.001, ****p<0.0001

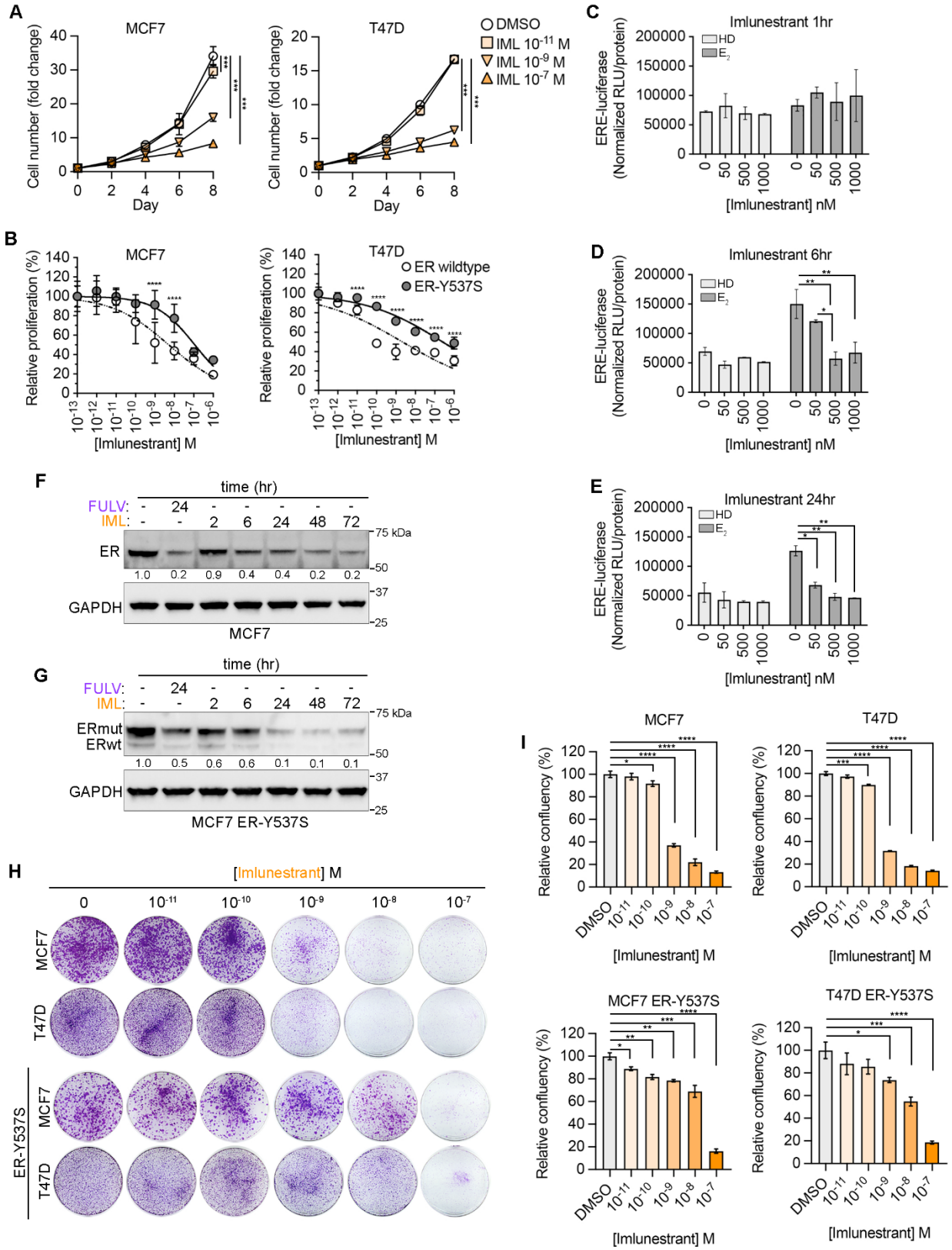
A
MCF7
T47D
Cell number (fold change)
Day
DMSO
IML 10-11 M
IML 10-9 M
IML 10-7 M
B
MCF7
T47D
Relative proliferation (%)
[Imlunestrant] M
ER wildtype
ER-Y537S
C
Imlunestrant 1hr
D
Imlunestrant 6hr
E
Imlunestrant 24hr
ERE-luciferase (Normalized RLU/protein)
HD
E2
[Imlunestrant] nM
F
time (hr)
FULV:
IML:
ER
GAPDH
75 kDa
50
37
25
MCF7
G
ERmut
ERwt
MCF7 ER-Y537S
H
[Imlunestrant] M
ER-Y537S
I
Relative confluency (%)
DMSO

Figure 2: Transcriptional effects of imlunestrant

A) Cartoon schematic of the RNAseq treatment conditions. **B)** Volcano plot of the differentially expressed genes following estradiol treatment or **C)** doxycycline-induction of ER-Y537S in MCF7 cells. Dotted lines denote chosen cutoffs |log2FC| >= 1 and FDR < 10%. Orange is upregulated and blue is downregulated following treatment. N = 2 replicates per group. ESR1 and estrogen-regulated genes are labeled with gene names when significant. **D)** Bar plot of the number of differentially expressed genes in MCF7 or **E)** T47D cells following IML or FULV treatment in cells expressing WT-ER or ER-Y537S. **F)** Dot plot of gene set testing results in ER-Y537S expressing cells for the Hallmark gene collection using cameraPR (10% FDR threshold per column).

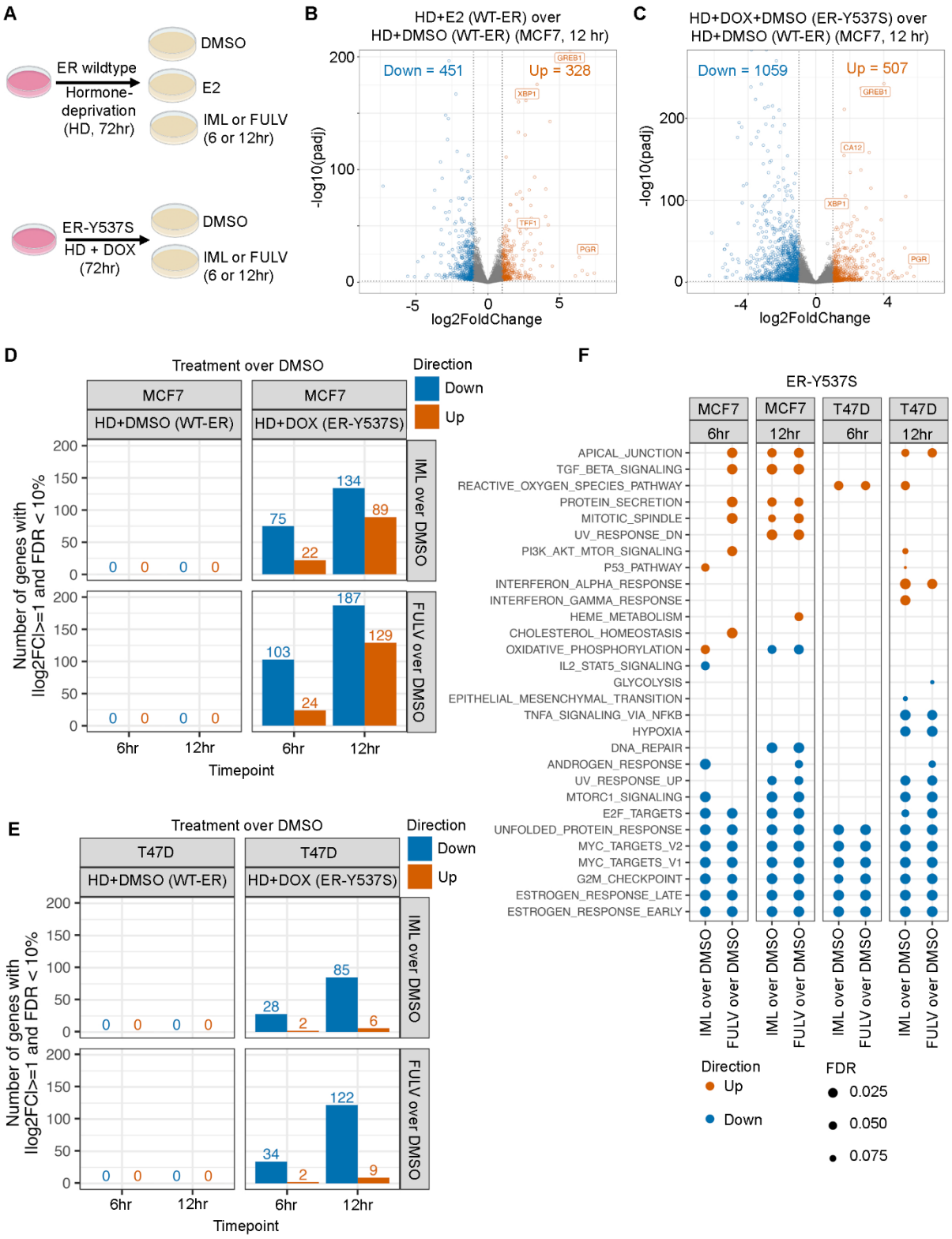
A
ER wildtype
Hormone-deprivation (HD, 72hr)
DMSO
E2
IML or FULV (6 or 12hr)
ER-Y537S
HD + DOX (72hr)
DMSO
IML or FULV (6 or 12hr)
B
HD+E2 (WT-ER) over HD+DMSO (WT-ER) (MCF7, 12 hr)
Down = 451
Up = 328
-log10(padj)
log2FoldChange
C
HD+DOX+DMSO (ER-Y537S) over HD+DMSO (WT-ER) (MCF7, 12 hr)
Down = 1059
Up = 507
-log10(padj)
log2FoldChange
D
Treatment over DMSO
Direction
Down
Up
MCF7
HD+DMSO (WT-ER)
HD+DOX (ER-Y537S)
IML over DMSO
FULV over DMSO
Number of genes with |log2FC|>=1 and FDR < 10%
Timepoint
6hr
12hr
E
Treatment over DMSO
T47D
HD+DMSO (WT-ER)
HD+DOX (ER-Y537S)
F
ER-Y537S
MCF7
T47D
6hr
12hr
APICAL_JUNCTION
TGF_BETA_SIGNALING
REACTIVE_OXYGEN_SPECIES_PATHWAY
PROTEIN_SECRETION
MITOTIC_SPINDLE
UV_RESPONSE_DN
PI3K_AKT_MTOR_SIGNALING
P53_PATHWAY
INTERFERON_ALPHA_RESPONSE
INTERFERON_GAMMA_RESPONSE
HEME_METABOLISM
CHOLESTEROL_HOMEOSTASIS
OXIDATIVE_PHOSPHORYLATION
IL2_STAT5_SIGNALING
GLYCOLYSIS
EPITHELIAL_MESENCHYMAL_TRANSITION
TNFA_SIGNALING_VIA_NFKB
HYPOXIA
DNA_REPAIR
ANDROGEN_RESPONSE
UV_RESPONSE_UP
MTORC1_SIGNALING
E2F_TARGETS
UNFOLDED_PROTEIN_RESPONSE
MYC_TARGETS_V2
MYC_TARGETS_V1
G2M_CHECKPOINT
ESTROGEN_RESPONSE_LATE
ESTROGEN_RESPONSE_EARLY
IML over DMSO
FULV over DMSO
Direction
Up
Down
FDR
0.025
0.050
0.075

Figure 3: Imlunestrant treatment leads to decreased proliferation and tumor regression

A) Tumor volumes of ER-Y537S PDX treated with vehicle (VEH, black), fulvestrant (FULV, purple), 5mg subcutaneously per week or imlunestrant 15mg/kg oral daily (IML, orange). Error bars denote ± standard deviation. Two-way ANOVA with Dunnett's multiple comparisons test. N = 3 mice/treatment on day 10 and N =5 mice/treatment on day 28. **B)** Body weight of the PDX-bearing mice treated with VEH, FULV, or IML. Error bars denote ± standard deviation. One ANOVA with Tukey's multiple comparisons test. **C)** Representative images of immunohistochemistry staining on ER-Y537S PDX day 10 for ER or PR or Ki67. **D)** IHC staining index for ER or **E)** PR or **F)** % Ki67 positive on ER-Y537S PDX day 10 tissue. Box and whisker plot with maximum and minimum. One way ANOVA with Tukey's multiple comparisons test, n = 2 mice, 4-5 images from each mouse. **G)** Representative images of IHC staining on ER-Y537S PDX tissue treatment day 28 stained for ER or PR or Ki67. 20X magnification, scale bar is 100 um. **H)** IHC staining index for ER or **I)** PR or **J)** % Ki67 positive on day 28 ER-Y537S PDX tissue. Box and whisker plot with maximum and minimum. One way ANOVA with Tukey's multiple comparisons test, n= 2 mice, 4-5 images from each mouse. *$p<0.05$, **$p<0.01$, ***$p<0.001$, ****$p<0.0001$.

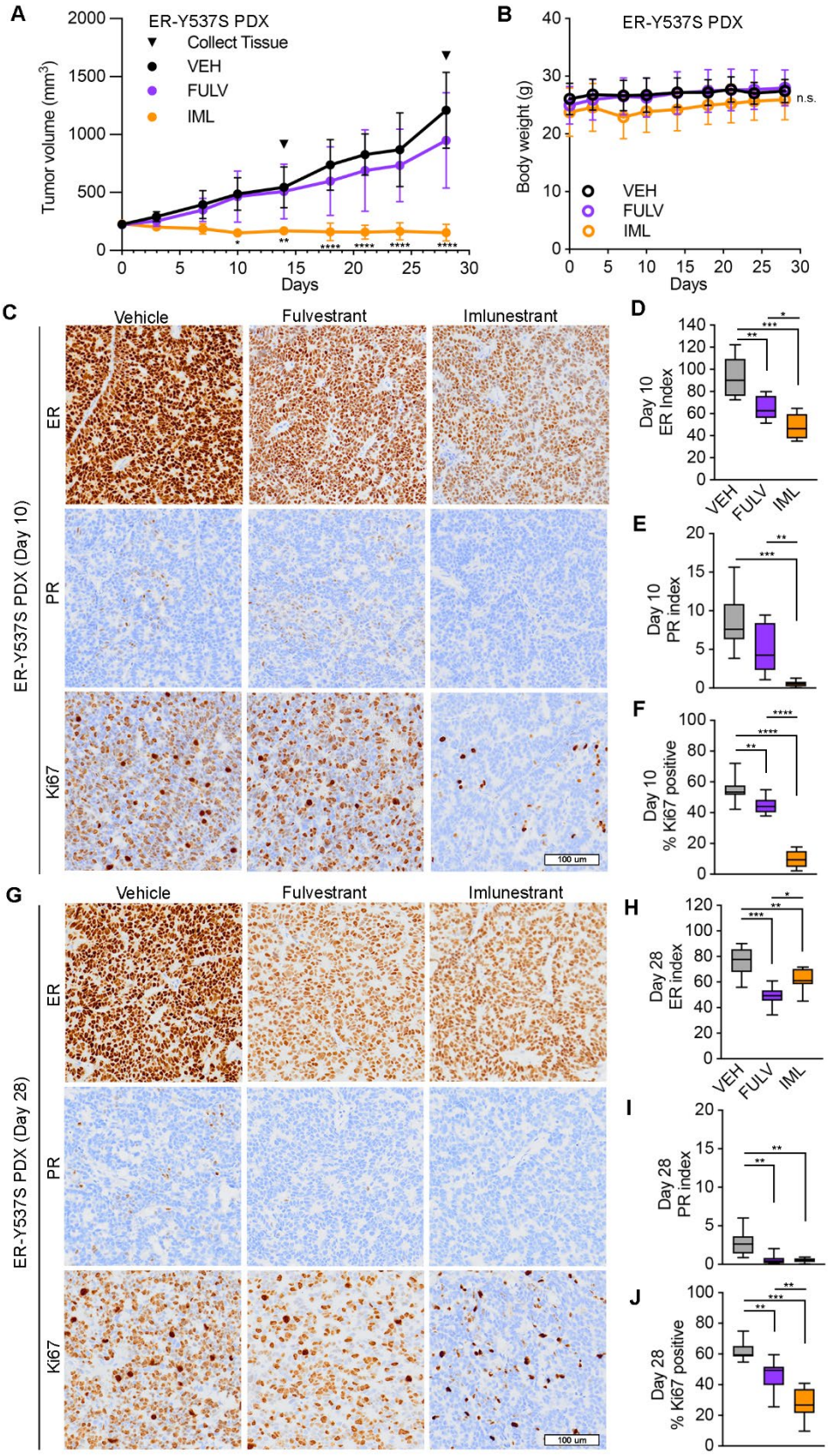
A
ER-Y537S PDX
Collect Tissue
VEH
FULV
IML
Tumor volume (mm3)
Days
B
ER-Y537S PDX
Body weight (g)
n.s.
VEH
FULV
IML
Days
C
Vehicle
Fulvestrant
Imlunestrant
ER
PR
Ki67
ER-Y537S PDX (Day 10)
100 um
D
Day 10 ER Index
VEH
FULV
IML
E
Day 10 PR index
F
Day 10 % Ki67 positive
G
Vehicle
Fulvestrant
Imlunestrant
ER
PR
Ki67
ER-Y537S PDX (Day 28)
100 um
H
Day 28 ER index
VEH
FULV
IML
I
Day 28 PR index
J
Day 28 % Ki67 positive

Figure 4: Multi-parametric immunofluorescence analysis

A) Representative immunofluorescence images for DAPI, Ki67, p21, Rb phosphorylated at Serines 807/811 (phospho-Rb), and merged staining from ER-Y537S patient-derived xenograft (PDX) treated for 10 days with vehicle, fulvestrant, or imlunestrant. N = 3 mice/treatment. Scale bar is 50 um. **B)** Multi-parametric immunofluorescence (MPI) quantification of proliferative fraction, non-proliferative fraction, and arrested fraction of epithelial cells after treatment with VEH (vehicle), FULV (fulvestrant) or IML (imlunestrant) for 10 days. Each point represents one mouse. Bar plot with average ± standard deviation. One way ANOVA with Tukey's multiple comparisons test. **C)** Representative immunofluorescent images after 28 days of treatment. N ≥ 4 mice/treatment. **D)** MPI quantification of immunofluorescence after treatment for 28 days. One way ANOVA with Tukey's multiple comparisons test. **E)** Pseudotime circle-fitted distribution of proliferative cells from ER-Y537S PDX tumors treated with VEH, FULV, or IML for 10 days or **F)** 28 days. Scatter plot, each point represents a cell with n ≥ 1,909 cells/treatment. Orange circle indicates G1 cell cycle arrest in IML treated tumors. *p<0.05, **p<0.01, ***p<0.001, ****p<0.0001.

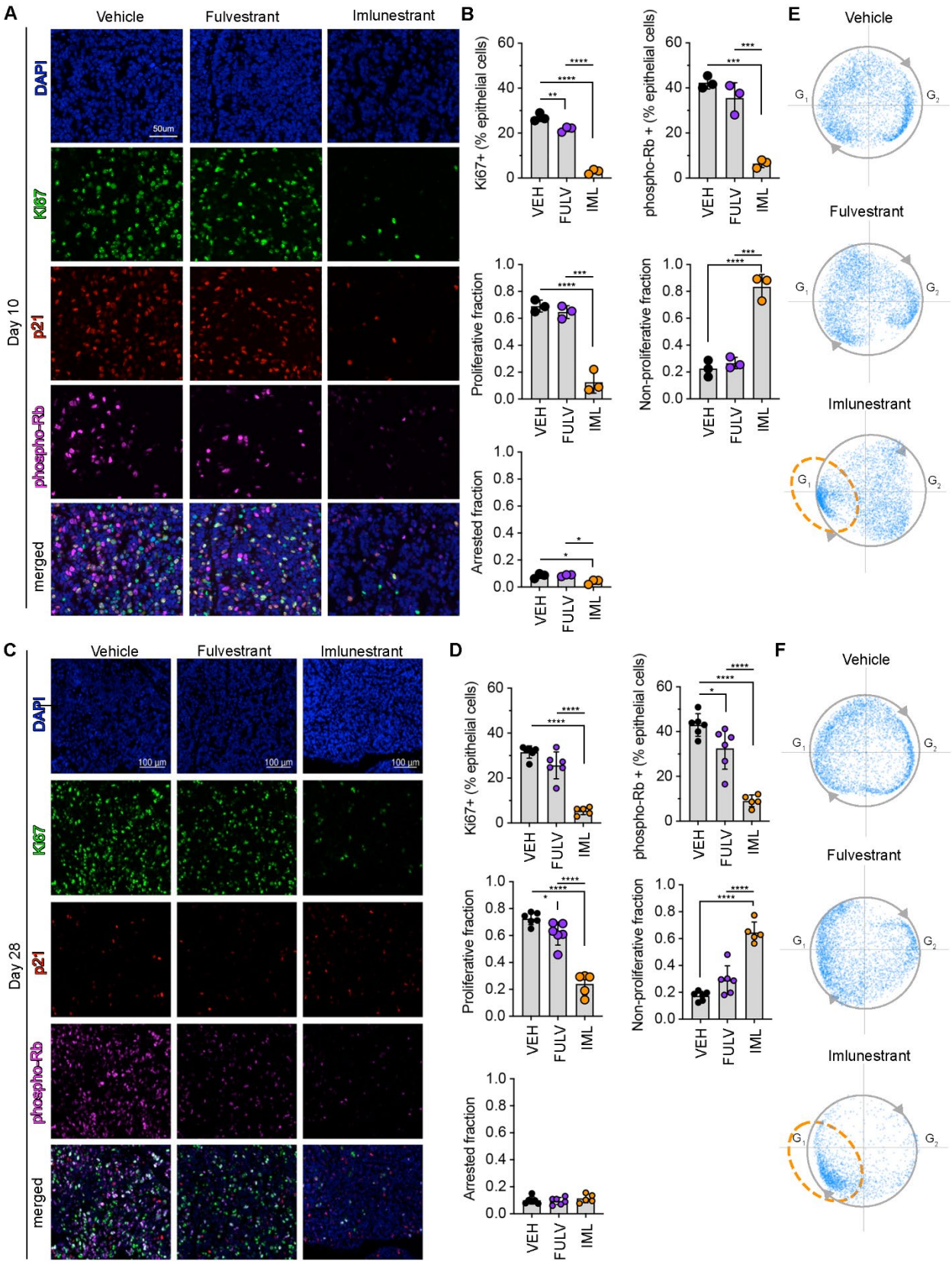
A
Vehicle
Fulvestrant
Imlunestrant
Day 10
DAPI
Ki67
p21
phospho-Rb
merged
50um
B
Ki67+ (% epithelial cells)
phospho-Rb + (% epithelial cells)
Proliferative fraction
Non-proliferative fraction
Arrested fraction
VEH
FULV
IML
C
Day 28
100 µm
D
E
Vehicle
Fulvestrant
Imlunestrant
G1
G2
F

Figure 5: Transcriptomic effects of imlunestrant

A) Bar plot of the number of differentially expressed genes in ER-Y537S patient-derived xenograft (PDX) treated with fulvestrant (FULV) or imlunestrant (IML) versus vehicle (VEH). Bars are orange for upregulated genes and blue for downregulated genes. Treatment duration for 10 days or 28 days. $N \geq 3$ mice per group. **B)** Heatmap of the row-centered variance-stabilized counts for the top 500 variable genes in ER-Y537S PDX tumors treated for 10 days with VEH, FULV, or IML. k-medoids clustering on 2 clusters with predominantly IML-downregulated genes and IML-upregulated genes following treatment for 10d or **C)** PDX treatment for 28d. **D)** Dot plot of gene set testing results for the Hallmark gene collection using cameraPR (10% FDR threshold per column). **E)** Imlunestrant (green) docked to x-ray crystal structure of the ER LBD harboring the Y537S mutation (PDB: 9bu1). Proximity to residues important for ligation (orange) reveals imlunestrant occupation of ligand binding pocket. **F)** Ligand binding pose comparison between imlunestrant and a derivative of the aliphatic SERD ICI 164,384 (PDB: 7r62, a derivative of estradiol that is closely related to fulvestrant) in cyan illustrates side arm conformation in relation to D351 (magenta) and S537 mutation (yellow).

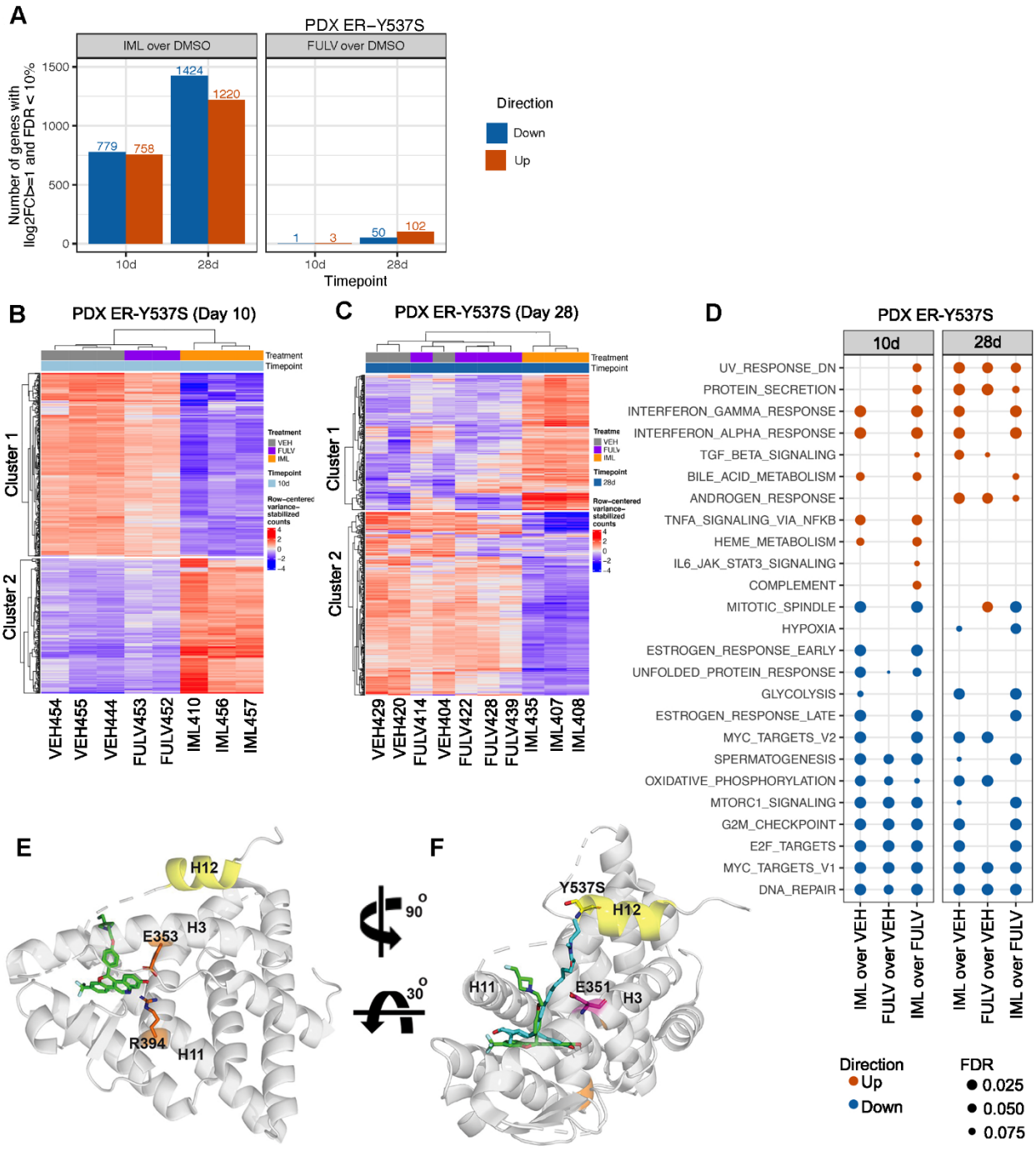
A
PDX ER−Y537S
IML over DMSO
FULV over DMSO
Number of genes with |log2FC|>=1 and FDR < 10%
1500
1000
500
0
779
758
1424
1220
1
3
50
102
10d
28d
Timepoint
Direction
Down
Up
B
PDX ER-Y537S (Day 10)
Treatment
Timepoint
Cluster 1
Cluster 2
VEH454
VEH455
VEH444
FULV453
FULV452
IML410
IML456
IML457
C
PDX ER-Y537S (Day 28)
VEH429
VEH420
FULV414
VEH404
FULV422
FULV428
FULV439
IML435
IML407
IML408
D
PDX ER-Y537S
10d
28d
UV_RESPONSE_DN
PROTEIN_SECRETION
INTERFERON_GAMMA_RESPONSE
INTERFERON_ALPHA_RESPONSE
TGF_BETA_SIGNALING
BILE_ACID_METABOLISM
ANDROGEN_RESPONSE
TNFA_SIGNALING_VIA_NFKB
HEME_METABOLISM
IL6_JAK_STAT3_SIGNALING
COMPLEMENT
MITOTIC_SPINDLE
HYPOXIA
ESTROGEN_RESPONSE_EARLY
UNFOLDED_PROTEIN_RESPONSE
GLYCOLYSIS
ESTROGEN_RESPONSE_LATE
MYC_TARGETS_V2
SPERMATOGENESIS
OXIDATIVE_PHOSPHORYLATION
MTORC1_SIGNALING
G2M_CHECKPOINT
E2F_TARGETS
MYC_TARGETS_V1
DNA_REPAIR
IML over VEH
FULV over VEH
IML over FULV
Direction
Up
Down
FDR
0.025
0.050
0.075
E
H12
H3
E353
R394
H11
90°
30°
F
Y537S
H12
H11
E351
H3

Figure 6: Genome wide CRISPR screen in the presence of imlunestrant treatment

A) Cartoon schematic of the genome-wide CRISPR/Cas9-knockout (KO) screen; 1) T47D cells are infected with the H3 lentiviral library of gRNAs, 2) infected cells are selected using puromycin, 3) cells are collected for untreated baseline (Day 0), or treated with DMSO or 1 nM imlunestrant, 4) after treatment for 14 or 31 days cells are collected, gRNAs amplified, and sequenced, followed by 5) gRNA analysis using MAGeCK algorithm. **B)** MAGeCK beta score and ranking results for gRNAs enriched or depleted after treatment with DMSO versus Day 0 for 14 days or **C)** 31 days. **D)** Mageck beta score and ranking results for gRNAs enriched or depleted after treatment with imlunestrant versus Day 0 for 14 days or **E)** 31 days. Scatter plot with each dot represents a gene in the genome-wide gRNA library, red are enriched after treatment (beta >/= +1), blue are depleted after treatment (beta </= -1), black are insignificant after treatment, genes in the ER pathway are orange, the CDK pathway are purple, and the MTORC1 pathway are green. **F)** Beta scores for individual genes depleted after imlunestrant treatment in the ER pathway, **G)** the CDK pathway, or **H)** the MTORC1 pathway.

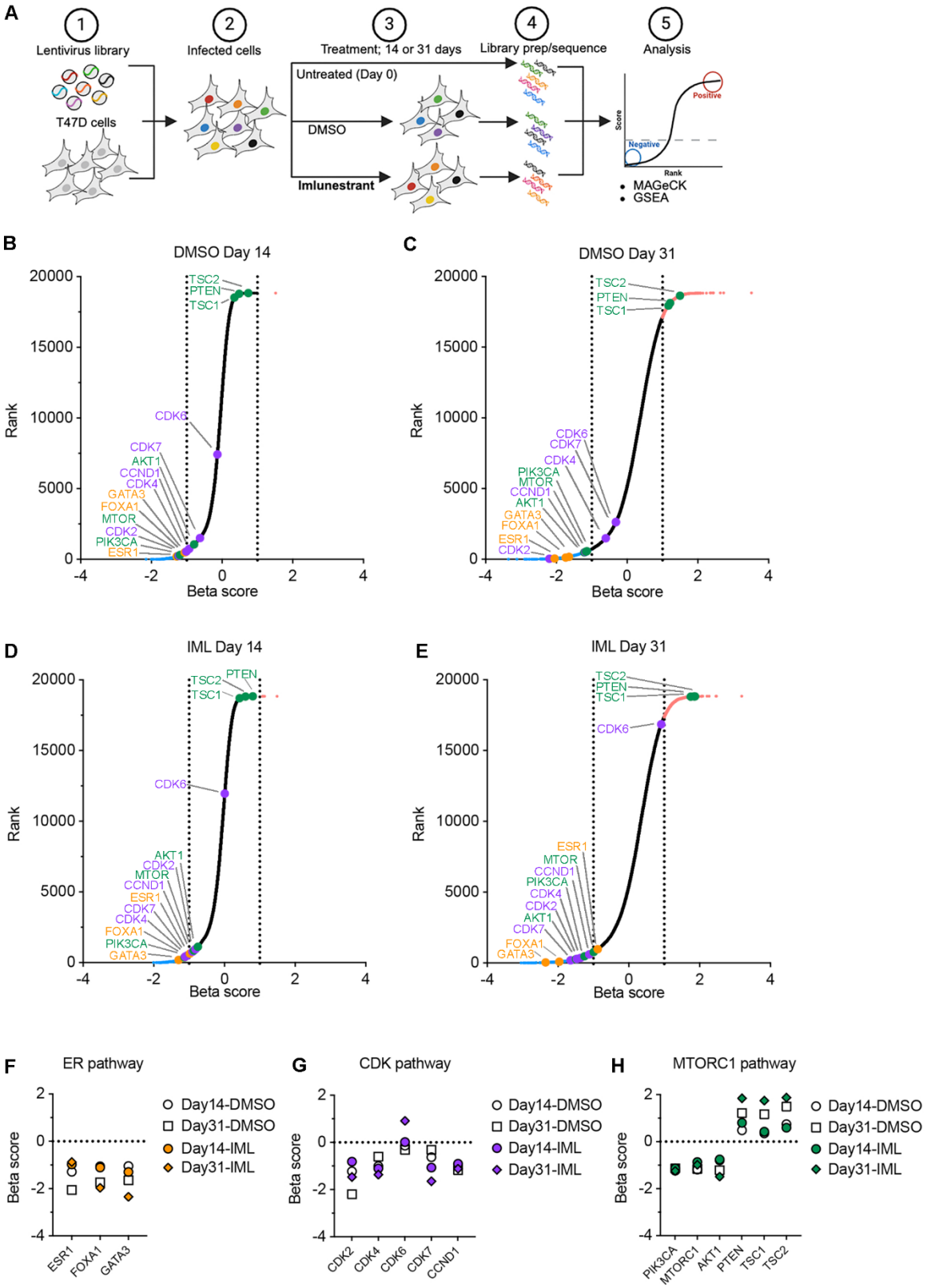
A
1
Lentivirus library
T47D cells
2
Infected cells
3
Treatment; 14 or 31 days
Untreated (Day 0)
DMSO
Imlunestrant
4
Library prep/sequence
5
Analysis
Positive
Negative
Score
Rank
MAGeCK
GSEA
B
DMSO Day 14
C
DMSO Day 31
D
IML Day 14
E
IML Day 31
Rank
Beta score
F
ER pathway
G
CDK pathway
H
MTORC1 pathway
Beta score
Day14-DMSO
Day31-DMSO
Day14-IML
Day31-IML
ESR1
FOXA1
GATA3
CDK2
CDK4
CDK6
CDK7
CCND1
PIK3CA
MTORC1
AKT1
PTEN
TSC1
TSC2

Figure 7: **Imlunestrant treatment increases the essentiality of genes related to oxidative phosphorylation**

A) Nine-square scatter plot of the gene beta scores in day 31 IML or day 31 DMSO treated T47D cells compared to day 0. Vertical and horizontal dotted lines denote +/- 1 standard deviation (SD) of DMSO or IML beta scores, respectively, and diagonal dotted lines denote +/- 1 SD of the difference in beta scores (IML – DMSO). Green are gRNAs enriched in only IML (IML up; IML beta score > 1 and DMSO beta score < 1) and orange are gRNAs depleted only in IML (IML down; IML beta score < -1 and DMSO beta score > -1 and < 1). **B)** Balloon plot of Hallmark GSEA results for genes in IML up or IML down. Circle size is the number of overlapping genes and circle color is the FDR q-value. **C)** Individual gene beta scores that are depleted in IML treated cells from the HALLMARK_OXIDATIVE_PHOSPHORYLATION and HALLMARK_REACTIVE_OXYGEN_SPECIES pathways. **D)** Fold change for MCF7 (left) or T47D (right) cells during treatment up to 8 days with DMSO, IACS (10 nM), IML (100 nM), or IACS and IML. Growth curve with average ± standard deviation. One way ANOVA with Tukey's multiple comparisons test. **E)** Normalized cell proliferation for MCF7 (circle) or T47D (square) cells expressing ER-Y537S and treated with a dose-response of IACS for 5 days. Growth curves with average ± standard deviation. Two way ANOVA with Sidak's multiple comparisons test. **F)** Synergy distribution analysis in MCF7 ER-Y537S cells treated with a dose response matrix of IACS and IML. Loewe synergy score using the synergyfinder tool. Red indicates synergism. **G)** Normalized cell proliferation for MCF7 parental (black) or MCF7 LTE-IML (orange) cells treated with IML (left) or IACS (right). Growth curve with average ± standard deviation. Two-way ANOVA with Sidak's multiple comparisons test. **H)** Colony assay crystal violet staining results from MCF7 parental or LTE-IML cells treated with imlunestrant (100 nM), IACS (10 nM), IML and IACS for two weeks in full media. **I)** Relative confluency of colony assay crystal violet

staining in H). Bar graph with average ± standard deviation. Two-way ANOVA with Dunnett's multiple comparisons test. *p<0.05, **p<0.01, ***p<0.001, ****p<0.0001.

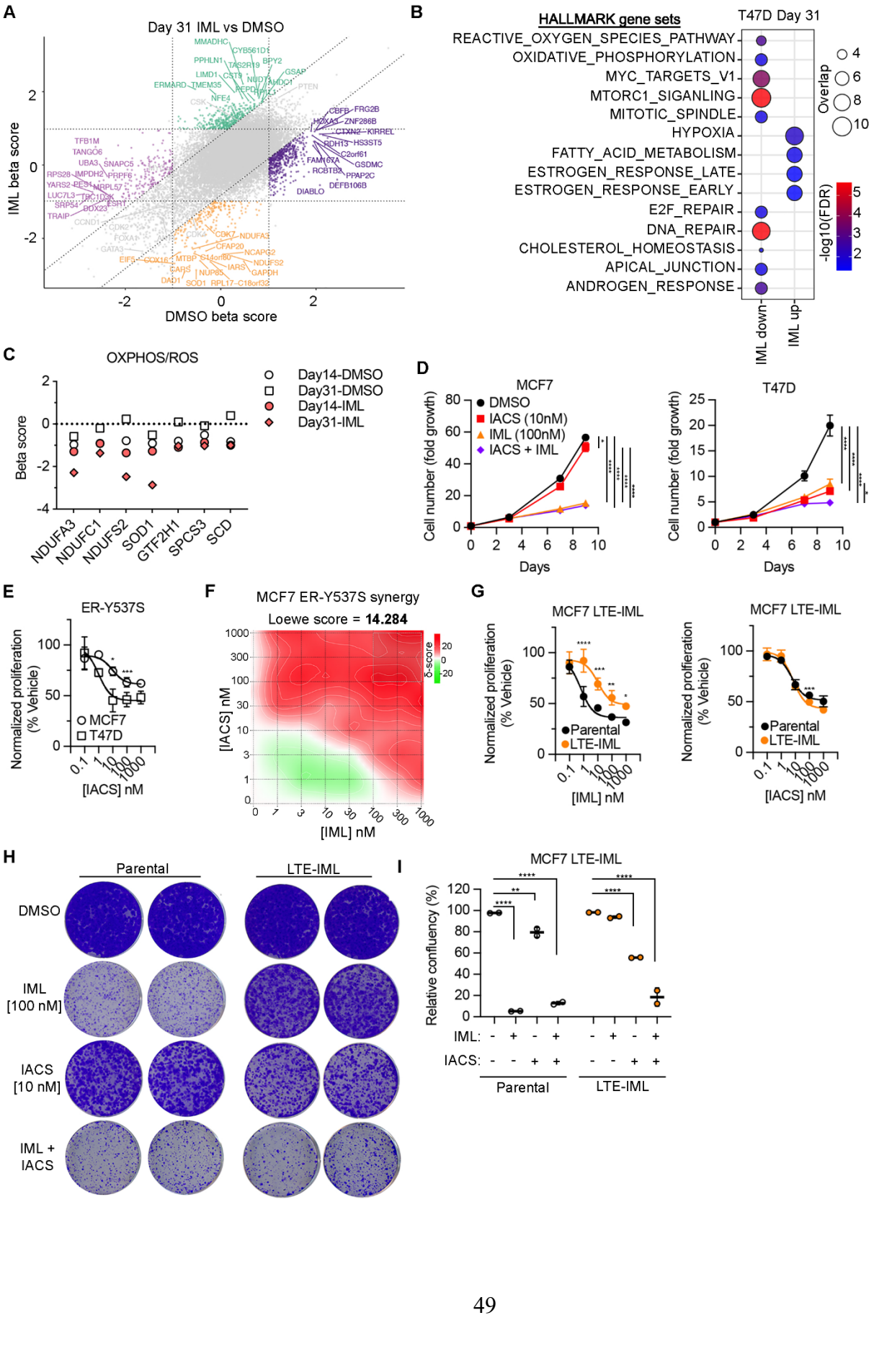
A
Day 31 IML vs DMSO
IML beta score
DMSO beta score
B
HALLMARK gene sets
T47D Day 31
REACTIVE_OXYGEN_SPECIES_PATHWAY
OXIDATIVE_PHOSPHORYLATION
MYC_TARGETS_V1
MTORC1_SIGANLING
MITOTIC_SPINDLE
HYPOXIA
FATTY_ACID_METABOLISM
ESTROGEN_RESPONSE_LATE
ESTROGEN_RESPONSE_EARLY
E2F_REPAIR
DNA_REPAIR
CHOLESTEROL_HOMEOSTASIS
APICAL_JUNCTION
ANDROGEN_RESPONSE
Overlap
-log10(FDR)
IML down
IML up
C
OXPHOS/ROS
Beta score
Day14-DMSO
Day31-DMSO
Day14-IML
Day31-IML
NDUFA3
NDUFC1
NDUFS2
SOD1
GTF2H1
SPCS3
SCD
D
MCF7
T47D
DMSO
IACS (10nM)
IML (100nM)
IACS + IML
Cell number (fold growth)
Days
E
ER-Y537S
Normalized proliferation (% Vehicle)
MCF7
T47D
[IACS] nM
F
MCF7 ER-Y537S synergy
Loewe score = 14.284
δ-score
[IACS] nM
[IML] nM
G
MCF7 LTE-IML
Normalized proliferation (% Vehicle)
Parental
LTE-IML
[IML] nM
[IACS] nM
H
Parental
LTE-IML
DMSO
IML [100 nM]
IACS [10 nM]
IML + IACS
I
MCF7 LTE-IML
Relative confluency (%)
IML:
IACS:
Parental
LTE-IML